OPEN ACCESS
IOP Publishing
Journal of Physics G: Nuclear and Particle Physics
J. Phys. G: Nucl. Part. Phys. **52** (2025) 035102 (16pp)
https://doi.org/10.1088/1361-6471/ada8c6

Study of proton-induced excitation functions on ^{nat}Ge up to 60 MeV

Arshiya Anees Ahmed, Ryszard Misiak, Jerzy W Mietelski, Kamil Brudecki and Barbara Marczewska

Institute of Nuclear Physics, Polish Academy of Sciences, Cracow, Poland

E-mail: arshiya.ahmed@ifj.edu.pl

Received 7 August 2024, revised 3 January 2025
Accepted for publication 10 January 2025
Published 30 January 2025

Abstract

The cross sections for the production of medically significant radioisotopes, including ^{68}Ge, ^{69}Ge, ^{66}Ga, ^{67}Ga, ^{72}As and various radioimpurities produced in pure germanium crystal irradiated with 60 MeV protons, were measured. The experiment utilized germanium targets with natural isotopic composition. Irradiation of the targets was performed using a proton beam from the AIC-144 accelerator at the Institute of Nuclear Physics, Polish Academy of Sciences, Krakow. Gamma spectroscopy was conducted with high-purity germanium detectors to measure the gamma-ray emissions from the irradiated targets. This enabled the determination of reaction cross-sections of the produced radionuclides. Additionally, our results were compared with existing literature and TALYS data to validate our findings. Generally, our experimental results align with previous studies, although discrepancies were observed in certain aspects. Specifically, nuclear model calculations and some literature data indicate slightly higher values compared to our findings.

Keywords: proton induced reactions, radio-generators, PET-tracers, radiopharmaceuticals, nat Ge

1. Introduction

The field of medicine has extensively leveraged the power of radioisotopes, with continuous efforts dedicated to discovering new radionuclides to improve production efficiency and

therapeutic effectiveness. Radiation and radioisotopes have gained significant attention for their applications in medical diagnostics and treatments, particularly in single photon emission computed tomography (SPECT) and positron emission tomography (PET). Short-lived tracers are preferred *in vivo* to minimize radiation exposure. Nonetheless, the limited availability of facilities and expertise in isotope production and medical diagnostics presents a significant challenge.

To address this, the development of radionuclide generators, especially for short-lived nuclides derived from longer-lived parents, has become a critical advancement [1]. Pioneering research at Brookhaven National Laboratory (BNL) led to the creation of groundbreaking systems such as the (^{90}Sr/^{90}Y) and (^{99}Mo/^{99m}Tc) generators, revolutionizing nuclear medicine by enabling portable generator systems for clinical use. The ^{99}Mo/^{99m}Tc generator remains a cornerstone of clinical nuclear medicine, utilized in approximately 80% of procedures. However, the primary production method via reactors faces significant challenges, as many reactors are scheduled for shutdown due to aging. In response, we are adopting accelerators for radioisotope production and developing alternative medical radionuclides as proposed solutions.

Globally, cancer remains a major public health issue, with rising incidence rates and associated mortalities. Projections indicate a continued increase in cancer cases and deaths by 2040, underscoring the urgent need for effective diagnostic and therapeutic interventions [2]. As cancer incidence rises, the demand for medical radionuclides also grows, necessitating continuous innovation and development of novel radioisotopes to enhance diagnostic accuracy and therapeutic efficacy [3].

The production of a radionuclide requires comprehensive knowledge of nuclear reaction cross sections. This data is essential for determining the optimum energy range for desired radionuclide production, calculating thick target yield, and assessing the level of isotopic radionuclidic impurities for a given thickness and enrichment of the target material.

Generally, neutron-spectrum averaged cross sections for (n, γ) and (n, p) reactions are available, though some uncertainties persist. In cyclotron production of radionuclides, the data requirements are more stringent compared to a nuclear reactor. Comprehensive knowledge of the excitation functions of the relevant nuclear reactions is necessary [4]. Numerous studies have explored the potential of producing novel radionuclide such as ^{66}Ga, ^{67}Ga, ^{68}Ge/^{68}Ga, ^{69}Ge and ^{72}As using proton accelerators [5–43]. However, the database is weak when it comes to employing germanium targets to study these radionuclides.

This study aims to enhance the database for improving cyclotron-based charged particle nuclear reaction predictions. We investigate the proton-induced reaction on natural germanium (^{nat}Ge) targets, exploring the medically important radionuclide and radioimpurity production excitation functions from the threshold up to 60 MeV proton energy.

2. Experimental details

2.1. Material and methods

Using a conventional stacked foil activation technique combined with gamma-ray spectrometry, we measured the excitation functions of proton-induced nuclear reactions on natural germanium (^{nat}Ge) as a function of proton energies from the threshold up to 60 MeV.

High-purity (99.99999%) natural germanium, supplied by Umicore N.V. (Belgium), was used as the target for proton irradiation. Ten germanium disks were employed in this study, each with a diameter of 8.0 $\pm$ 0.1 mm. The thickness of the first six targets was 1.05 $\pm$ 0.04 mm, while the subsequent targets had a thickness of 0.48 $\pm$ 0.05 mm. The

Table 1. Mass spectrometer operating conditions.

Acquisition mode	MS/MS (dual mode)
RF power [W]	1550
Sampling depth [mm]	8
Gas flow rate [l min^{-1}]	1.07
Make-up gas flow rate [l min^{-1}]	0
Spray chamber temperature [°C]	2
He cell gas flow rate [ml min^{-1}]	4.5

Table 2. Isotopic composition of natural germanium [%].

Isotope	70	72	73	74	76
This work	19.59	26.91	7.67	37.54	8.29
IUPAC recommendation [44]	20.52	27.45	7.76	36.52	7.75

germanium target thicknesses were selected to ensure uniform energy deposition and minimize energy straggling within the stack. This configuration allowed for a high-resolution measurement of excitation functions across a wide proton energy range.

The natural germanium abundances were determined by using a triple quadrupole inductively coupled plasma mass spectrometer (Agilent 8900). The spectrometer was operated in collision-reaction mode, with a helium flow of 4.5 ml per minute, and in MS/MS mode. The exact operating parameters of the spectrometer are described in table 1. To achieve optimal measurement precision, germanium isotope ratios were measured at least 100 times. Quality control was conducted by using natural germanium with well-known abundances. The isotopic composition of germanium obtained in this study was compared with the values recommended by the International Union of Pure and Applied Chemistry (IUPAC) (see table 2).

The target stack was assembled in two configurations: three sets as Al–Cu–Ge and the remaining sets as Cu–Ti–Ge, covering the proton energy range of 14–60 MeV. High-purity (99.9%) metallic thin foils of natural aluminum (Al), copper (Cu), and titanium (Ti) served as beam monitors [45], each with a thickness of 10 ± 0.1 μm. The use of high-purity aluminum, copper, and titanium foils as beam monitors was based on their well-documented reaction cross-sections in the energy range of interest. The entire target sets were assembled in an aluminum target holder for irradiation.

The stacked target system was irradiated at the AIC-144 cyclotron of the Henryk Niewodniczański Institute of Nuclear Physics, Polish Academy of Sciences, in Cracow, Poland. The irradiation was performed continuously for 5 h and 15 min with a proton beam energy of 60.5 ± 0.5 MeV. The average beam current, determined from the monitoring foils, was 18.5 ± 1.1 nA. The gamma spectroscopy was started 18 h after the end of irradiation.

2.2. Detector setup and measurements

The activity of the irradiated targets was measured using a co-axial p-type high-purity germanium detector, which has a 10% relative efficiency and an energy resolution of 3.4 keV FWHM at the 1332.5 keV peak of ^{60}Co. This detector was coupled with an ORTEC Multichannel Analyzer 919E Ether-NIM.

Energy and efficiency calibrations of the detector were performed using standard sources such as ^{22}Na, ^{60}Co, ^{88}Y, ^{109}Cd, ^{137}Cs, ^{133}Ba, and ^{241}Am. Routine energy calibration was controlled using a ^{152}Eu source. The detector was calibrated for various sample-detector geometries, ensuring that activity measurements were performed within one of these calibrated geometries, thereby eliminating the need for efficiency function interpolation. Throughout the measurements, careful monitoring ensured the detector's dead time remained below 5% to avoid pile-up effects. The photopeak area of the spectra was determined using the CERN-developed software, Root: A data analysis framework [46]. For the analysis of all identified radioisotopes, we referred to nuclear data from the following databases: [47–49].

Each irradiated target from the stack was measured multiple times, following the data analysis methods described in previous works [50]. The SRIM and Geant4 software were used to estimate the energy degradation along the stacks and the corresponding particle energy at the center of each foil. The energy range within the target spanned from 1.7 to 2.8 MeV. The mean energy inside the target and the associated energy spread are provided in table 4.

Thin metal foils of Al, Cu, and Ti were used to determine the beam current and energy. The induced activity in each monitoring foil (positioned in front of the Ge target) was measured for the following reactions: ^{nat}Al(p, x)^{22,24}Na, ^{nat}Cu(p, x)^{56}Co,^{62,65}Zn and ^{nat}Ti(p, x)^{48}V [45]. The beam current was found to be consistent through the stack, with a mean value of 18.5 $\pm$ 1.1 nA.

Various sources of uncertainty were considered to estimate the uncertainty in the measured reaction cross-section and production yield values. These included statistical error (5%–8%), error in monitor reactions and nuclear data (6%), error in sample thickness (2%), error in detector efficiency calibration (5%), and error associated with beam energy and current estimation (5%). The overall uncertainty for the reaction cross-section was approximately in the range 9%–11%. The quadratic sum of these uncertainties was used to determine the total level of uncertainty.

3. Results and discussion

Table 3 presents the nuclear data for all radionuclides studied in this work, including the radioimpurities. The aim of this article is to study the production of medically promising radionuclides using ^{nat}Ge target and contribute to the enhancement of nuclear database.

The cross sections for all those studied radioisotopes in this study from ^{nat}Ge(p,x) reactions are shown in table 4. The results were compared with published literature and TALYS (Version 2.0) predictions [51], which rely on nuclear reaction models incorporating global optical potentials and nuclear level densities. Figures 1–9 graphically represent these comparisons. The literature data were collected from the EXFOR database [52], which compiles experimental nuclear reaction data from various international studies to provide a comprehensive resource for cross-section validation.

3.1. Ga radionuclide

Gallium-66 (^{66}Ga, $T_{1/2} = 9.49$ h) is a short-lived radioisotope used in PET imaging and belongs to a category of isotopes with a relatively lower β^+ abundance (57%) [8, 53]. Several experiments have been conducted to study the production of ^{66}Ga using Zn and Cu targets. Very few studies have been conducted using Ge target; table 3 lists all the reactions contributing to the production of ^{66}Ga. Figure 1 present the cross-sections measured on Ge targets with natural isotopic abundance, along with our results and TALYS predictions. Our results

Table 3. Nuclear data for radionuclides produced via proton-induced reactions in a ^{nat}Ge target. Presented gamma-ray energies are used in the analysis. Uncertainties of the half-life, photon energies and the corresponding intensities in the last valid digits are in italics.

Radio nuclei	$T_{1/2}$	E_γ (keV)	I_γ (%)	Contributing reactions	Q-values (MeV)
^{65}Zn	243.93 d *8*	1115.539 *4*	50.04 *10*	^{70}Ge(p,$d\alpha$)	−12.92
				^{72}Ge(p,$nt\alpha$)	−24.83
				^{73}Ge(p,$2nt\alpha$)	−31.61
				^{74}Ge(p,$3nt\alpha$)	−41.81
				^{65}Ga decay	
^{66}Ga	9.49 h *3*	1039.220 *3*	37.0 *20*	^{70}Ge(p,$n\alpha$)	−10.04
				^{72}Ge(p,$3n\alpha$)	−28.21
				^{73}Ge(p,$4n\alpha$)	−34.99
				^{74}Ge(p,$5n\alpha$)	−45.19
^{67}Ga	3.2617 d *5*	93.310 *5*	38.81 *3*	^{70}Ge(p,α)	1.18
		184.576 *10*	21.410 *10*	^{72}Ge(p,$2n\alpha$)	−16.98
		300.217 *10*	16.64 *12*	^{73}Ge(p,$3n\alpha$)	−23.76
				^{74}Ge(p,$4n\alpha$)	−33.96
^{68}Ge	270.95 d *16*	No γ		^{70}Ge(p,t)	−11.24
		1077.34 *5*[a]	3.0	^{72}Ge(p,$2nt$)	−29.41
				^{73}Ge(p,$3nt$)	−36.19
				^{74}Ge(p,$4nt$)	−46.38
^{69}Ge	39.05 h *10*	574.11 *10*	13.3 *18*	^{70}Ge(p,d)	−9.31
		1106.77 *10*	36	^{72}Ge(p,nt)	−21.21
				^{73}Ge(p,$2nt$)	−28.00
				^{74}Ge(p,$3nt$)	−38.19
				^{76}Ge(p,$5nt$)	−54.12
^{71}As	65.30 h *7*	174.954 *5*	82.45 *22*	^{70}Ge(p,γ)	4.62
				^{72}Ge(p,$2n$)	−13.54
				^{73}Ge(p,$3n$)	−20.32
				^{74}Ge(p,$4n$)	−30.52
				^{76}Ge(p,$6n$)	−46.55
^{72}As	26.0 h *1*	629.92 *5*	8.07 *24*	^{72}Ge(p,n)	−5.13
				^{73}Ge(p,$2n$)	−11.92
				^{74}Ge(p,$3n$)	−22.11
				^{76}Ge(p,$5n$)	−38.05
^{73}As	80.30 d *6*	53.437 *9*	10.6 *11*	^{72}Ge(p,γ)	5.65
				^{73}Ge(p,n)	−1.12
				^{74}Ge(p,$2n$)	−11.32
				^{76}Ge(p,$4n$)	−27.25
^{74}As	17.77 d *2*	595.83 *8*	59 *3*	^{73}Ge(p,γ)	6.85
		634.78 *8*	15.4 *10*	^{74}Ge(p,n)	−3.34
				^{76}Ge(p,$3n$)	−19.27

In the provided table, d and t represent deuteron and triton particles, respectively.
[a] Cross sections determined through decay of ^{68}Ga.

Table 4. Experimentally determined cross sections of production of all the detected radioisotopes through the (p, x) reactions in a ^{nat}Ge target.

Proton energy (MeV)	Production cross section [mb] of different nuclei from the ^{nat}Ge(p,x) reactions								
	^{65}Zn	^{66}Ga	^{67}Ga	^{68}Ge	^{69}Ge	^{71}As	^{72}As	^{73}As	^{74}As
14.6 ± 2.3	–	–	8.03 ± 0.72	–	13.6 ± 1.2	20.5 ± 1.8	141 ± 14	128 ± 14	152 ± 15
19.5 ± 1.8	–	–	3.90 ± 0.35	–	53.8 ± 4.9	6.9 ± 0.6	68.6 ± 6.9	320 ± 35	77.2 ± 7.7
23.9 ± 1.9	–	–	7.94 ± 0.72	–	142 ± 13	124 ± 11	72.9 ± 7.3	229 ± 25	42.6 ± 4.3
28.1 ± 1.7	–	–	4.31 ± 0.39	20.7 ± 2.1	127 ± 11	108.5 ± 9.8	157 ± 16	122 ± 14	44.9 ± 4.5
33.1 ± 2.9	6.17 ± 0.68	7.47 ± 0.67	10.97 ± 0.99	69.6 ± 7.2	96.1 ± 8.7	82.4 ± 7.4	159 ± 16	51.9 ± 5.7	54.7 ± 5.5
39.1 ± 2.6	16.8 ± 1.8	4.40 ± 0.40	24.6 ± 2.2	94.5 ± 9.5	93.6 ± 8.4	58.5 ± 5.3	116 ± 11	47.5 ± 5.2	36.7 ± 3.7
44.6 ± 2.5	20.3 ± 2.2	6.05 ± 0.54	36.5 ± 3.3	71.5 ± 7.2	103.2 ± 9.3	60.3 ± 5.4	70.1 ± 7.1	45.3 ± 5.1	22.4 ± 2.2
49.7 ± 2.1	12.5 ± 1.4	–	55.4 ± 5.1	44.1 ± 4.4	118 ± 11	67.2 ± 6.1	44.9 ± 4.5	58.4 ± 6.4	16.7 ± 1.7
54.2 ± 2.1	9.3 ± 1.0	9.02 ± 0.81	134 ± 12	56.8 ± 5.7	123 ± 11	66.9 ± 5.8	38.8 ± 3.9	31.1 ± 3.4	13.8 ± 1.4
58.4 ± 1.8	11.5 ± 1.3	–	32.5 ± 2.9	51.9 ± 5.2	102.0 ± 9.2	47.4 ± 4.3	41.7 ± 4.2	–	14.2 ± 1.4

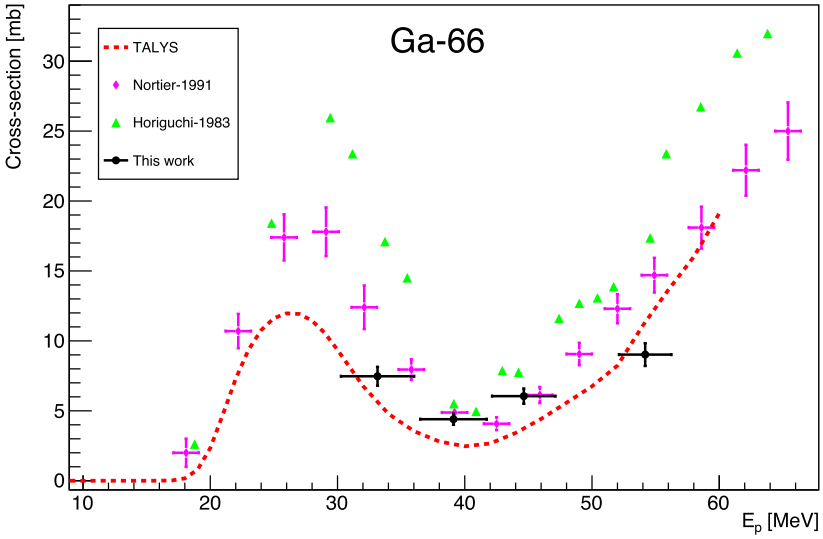

Figure 1. Excitation function of the ^{nat}Ge(p,x)^{66}Ga reaction.

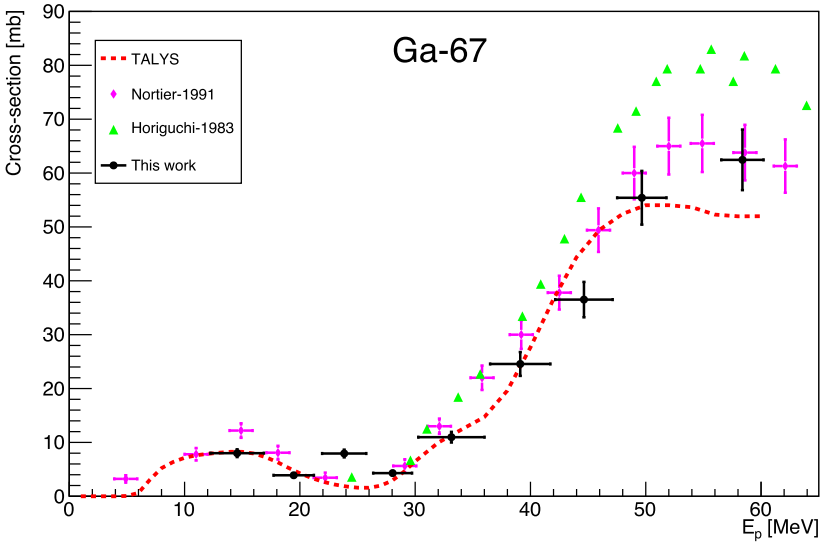

Figure 2. Reaction cross section of the ^{nat}Ge(p,x)^{67}Ga.

are in good agreements with the findings of [17] in the 30–50 MeV energy range, whereas data from [37] follow a similar excitation function trend but with higher magnitude. TALYS predictions underestimate the magnitude but accurately describe the trend of excitation function.

The metallic radionuclide Gallium-67 (^{67}Ga, $T_{1/2} = 3.26$ d) forms strong metal complexes and is of significant interest in diagnostic nuclear medicine, particularly for tumor detection and therapy. Extensive research has been conducted on targetry and chemical processing issues. For small-scale production, the (p, n) reaction on ^{67}Zn is commonly used

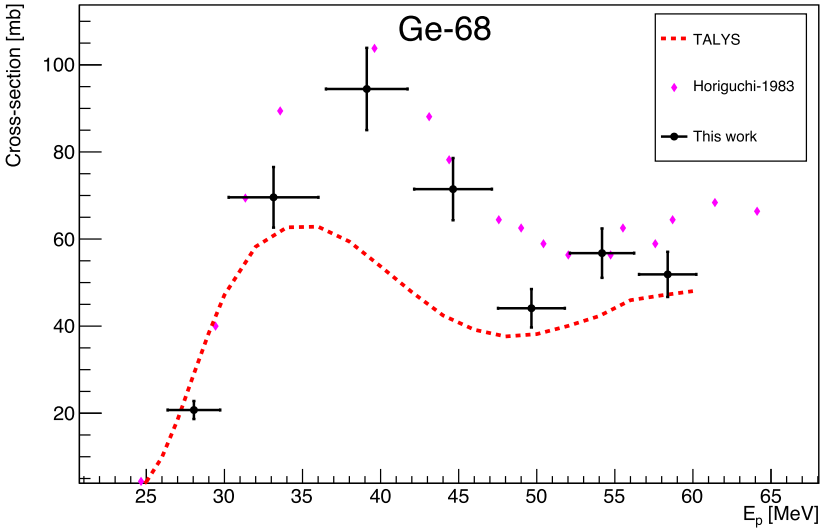

Figure 3. ^{68}Ge radioisotopes production cross-section through ^{nat}Ge(p,x) reactions.

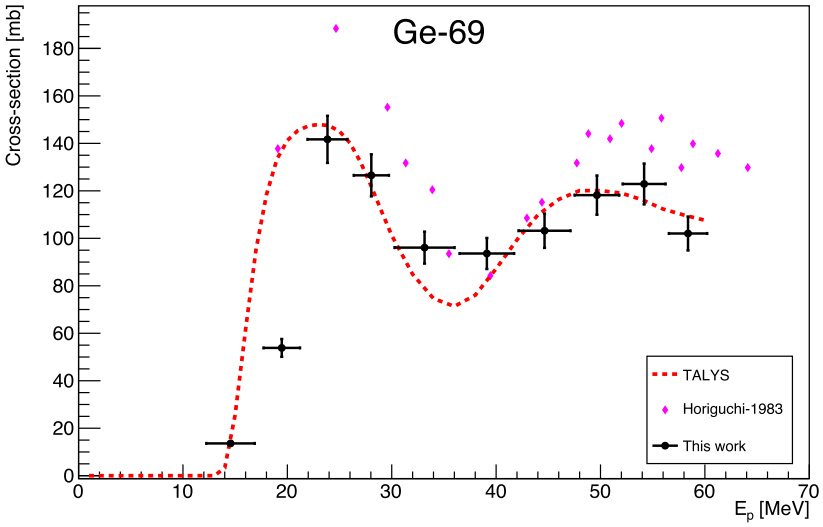

Figure 4. Measured excitation function of the ^{nat}Ge(p,x)^{69}Ge reaction.

[15]. ^{67}Ga emits several gamma rays at varying energies (93.31, 184.577, and 300.21 keV). Activities were evaluated using these gamma lines, and the average of the individual values was calculated. The reactions contributing to the production of ^{67}Ga over the investigated proton energy range are given in table 3. The previously reported data ([17, 37], TALYS predictions, and the results from this study is presented in figure 2. Our results demonstrate reasonably good agreement with both previous experimental data and theoretical calculations.

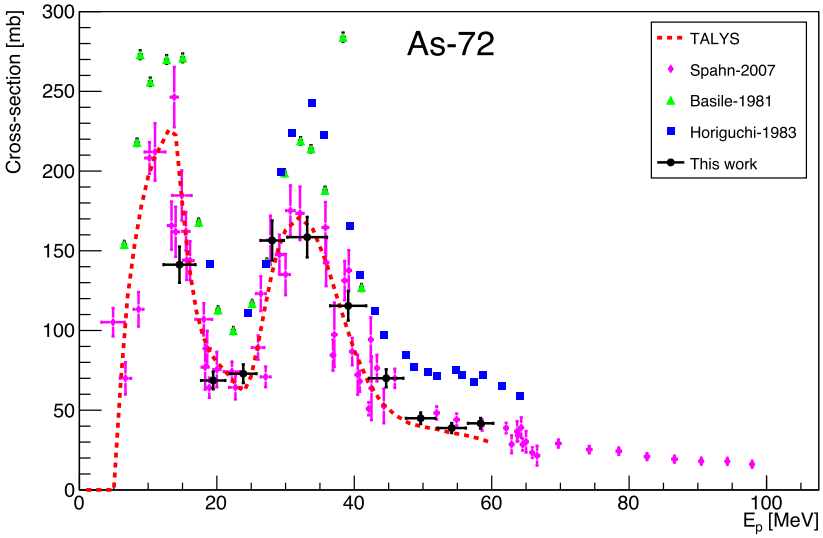

Figure 5. Excitation function of the ^{nat}Ge(p,x)^{72}As reaction.

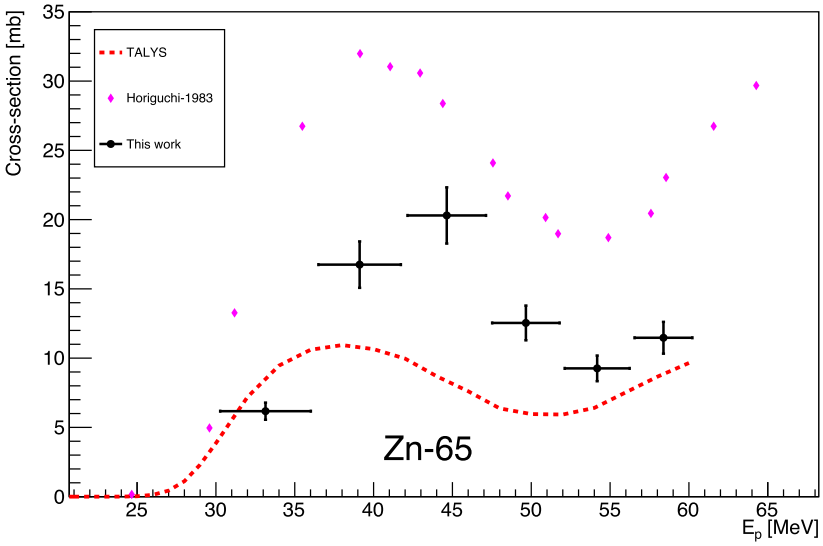

Figure 6. Excitation function of the ^{nat}Ge(p,x)^{65}Zn reactions.

3.2. Ge radionuclide

The long-lived isotope Germanium-68 (^{68}Ge, $T_{1/2} = 270.8$ d), which does not emit gamma radiation, was evaluated by measuring its short-lived daughter Gallium-68 through prolonged measurements (lasting at least 20 h) conducted weeks after the end of bombardment using 1077.35 keV gamma photon. The ^{68}Ge/^{68}Ga radionuclide generator is well-studied and widely used in medical applications. The formation of the ^{68}Ge isotope occurs through ^{70,72,73,74}Ge(p,x) reactions within the investigated proton energy range. Figure 3 present our

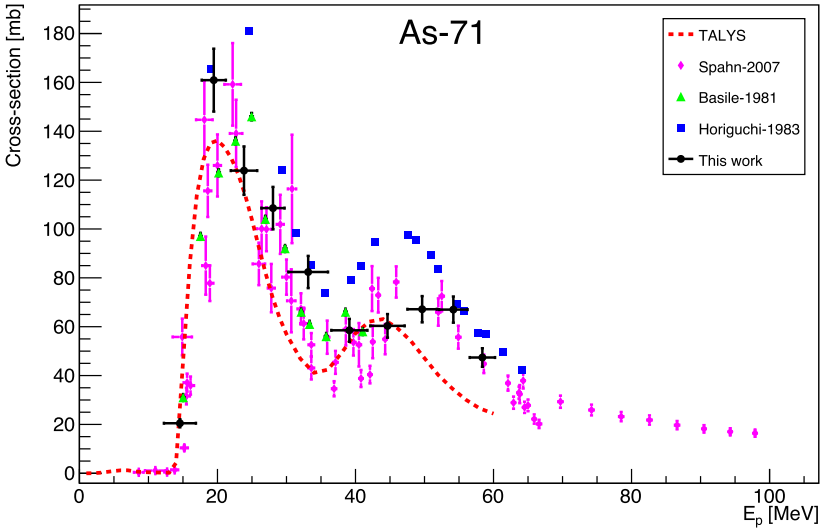

Figure 7. Measured excitation function of the ^{nat}Ge(p,x)^{71}As reaction.

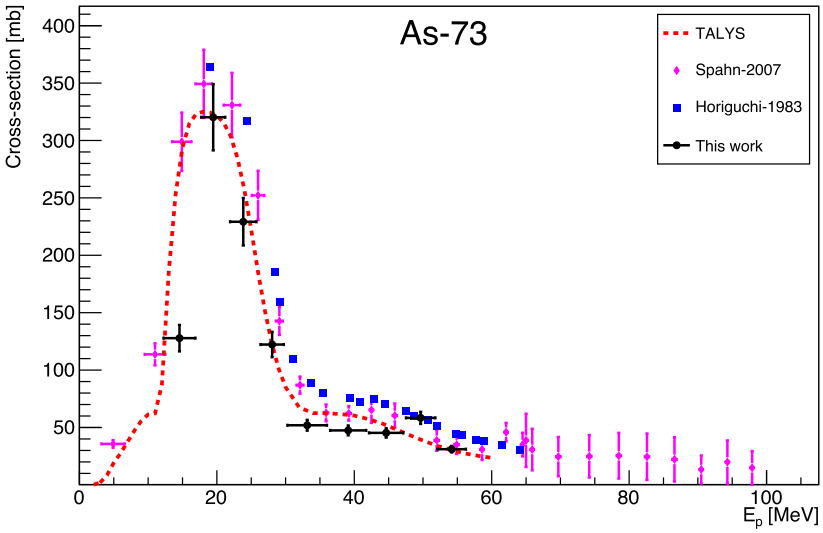

Figure 8. Excitation function of the ^{nat}Ge(p,x)^{73}As reaction.

results along with TALYS predictions and data from the only available experimental study in the literature [37]. Our data align well with the literature values.

Theoretical predictions from TALYS exhibit a similar shape but with a lower magnitude and a slight shift toward lower energy, particularly above the 37 MeV proton energy. This underestimation is likely due to limitations in the nuclear reaction models employed in TALYS. Specifically, TALYS relies on generalized nuclear level density parameters, which may not accurately reflect the structure of intermediate-mass isotopes like germanium. Furthermore, the calculation of pre-equilibrium contributions and gamma decay widths in TALYS may introduce additional deviations. The scarcity of experimental data for ^{68}Ge

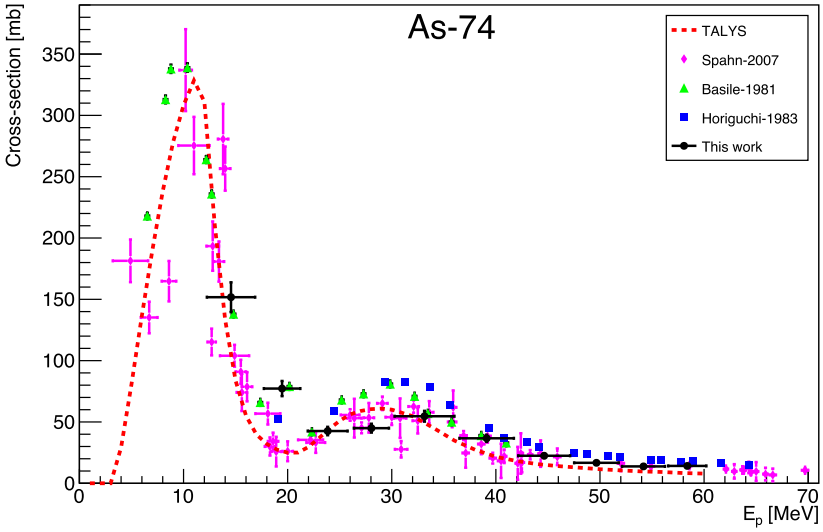

Figure 9. Reaction cross section of the ^{nat}Ge(p,x)^{74}As reaction.

production also limits the calibration and refinement of theoretical models, contributing to the observed discrepancies.

The production cross-sections for Germanium-69 (^{69}Ge, $T_{1/2} = 39.05$ h) were determined by measuring the 1106.7 keV gamma line ($I_\gamma = 36\%$) following a one-day cooling period. This radioisotope is a promising candidate for use as a PET tracer due to its β^+ decay and favorable half-life. Figure 4 illustrates the excitation function of the ^{nat}Ge(p,x)^{69}Ge reaction, comparing it with previously reported experimental data [37] and TALYS predictions. Our results are consistent with the TALYS predictions but are slightly lower than the values reported in the literature [37].

3.3. ^{72}As radioisotope

Arsenic-72 (^{72}As) is a notable radionuclide for PET imaging due to its strong β^+ emission, appropriate half-life, and optimal positron energy. The radionuclide is typically obtained through the ^{72}Se/^{72}As generator system [38, 54–56]. Direct production from a Germanium target has also been investigated, but the fundamental nuclear reaction cross-section data remain poorly understood. The cross-section data for the ^{nat}Ge(p,xn)^{72}As reaction are presented in figure 5, showing two peaks at approximately 12 and 32 MeV. These peaks correspond to the ^{72}Ge(p,n)^{72}As and ^{74}Ge(p,$3n$)^{72}As reactions, respectively [38]. The measured excitation function aligns well with the literature data [38], although the values reported by [37] and [36] are significantly higher. The theoretical curve derived from the TALYS calculation also shows good agreement with our results.

3.4. Radio impurities

Radioisotopes produced in this study, apart from those significant for medical applications, are classified as radioimpurities. However, many of these radionuclides have valuable applications in other fields, such as environmental studies and industrial applications.

The decay properties of ^{65}Zn ($T_{1/2} = 244.26$ d) make it ideal as a tracer in thin layer activation (TLA) studies. The TLA technique requires knowledge of the excitation function to

determine the depth distribution of the long-lived ^{65}Zn radionuclide. ^{65}Zn is formed via the ^{nat}Ge(p,x) reactions and ^{nat}Ge(p,x)^{65}Ga decay. The cumulative cross-sections for the formation of ^{65}Zn are presented in figure 6, along with available experimental data [37] and TALYS calculations for comparison. Our results do not align with TALYS and [37] data above 38 MeV proton energy. This divergence could be influenced by experimental factors such as energy degradation in the stacked foil setup or uncertainties in gamma spectroscopy measurements of the decay chains. Additionally, the cumulative production of ^{65}Zn through the decay of precursor isotopes like ^{65}Ga adds complexity, as the decay contribution may vary depending on experimental conditions and measurement timelines.

Arsenic plays a significant role in environmental and toxicological sciences [38, 57]. For tracer studies in these fields, the radionuclides ^{74}As with a $T_{1/2} = 17.77$ d have been suggested [36]. The ^{73}As ($T_{1/2} = 80.30$ d) is considered more suitable for environmental studies than ^{74}As due to its longer half-life and softer emitted radiation, which poses less of a radiation hazard. Table 3 summarizes all possible reactions contributing to the production of arsenic radionuclides within the proton energy range investigated in this study. Figure 7 presents the cross sections for the formation of ^{71}As. Two distinct maxima at approximately 20 and 50 MeV proton energy are observed. Our results follow the same trend as previous literature data [36–38] and exhibit good agreement. The data from [37] are slightly higher. The TALYS calculations generally follows the shape of the excitation function but underestimate the cross sections.

The excitation function of the ^{nat}Ge(p,xn)^{73}As reaction is depicted in figure 8. A major peak at approximately 20 MeV is observed. We have compared our data with the available experimental data [37, 38], along with the results of the TALYS calculation and our data agree well.

Figure 9 illustrates the results of the ^{nat}Ge(p,xn)^{74}As reaction, showing a prominent peak at approximately 10 MeV attributed to the ^{74}Ge(p,n)^{74}As reaction. Our results align well with the literature data [38]. The TALYS code accurately estimates the height and shape of the excitation function; however our measurements deviate from the calculated data around 20 MeV. Our data show a slightly smaller peak compared to the results of [36] and [37] in the 25–35 MeV proton energy range.

4. Conclusions

Nuclear reactions were investigated for a proton beam energy range of 14–60 MeV. We measured the cross sections for the production of medically relevant radioisotopes ^{66,67}Ga, ^{68,69}Ge, and ^{72}As, as well as radioimpurities ^{65}Zn and ^{71,73,74}As, using the stacked foil technique on ^{nat}Ge with a proton beam from the AIC-144 cyclotron at the Institute of Nuclear Physics of the Polish Academy of Sciences in Cracow. The measured cross sections were compared with available literature data.

For ^{67}Ga isotopes and all the arsenic radioisotopes considered in this study, we found good agreement within the bounds of uncertainty with most data sets, including TALYS predictions. However, for ^{65}Zn, neither the literature data nor TALYS predictions matched our results. For the ^{68}Ge radionuclide, our results agreed with the only available experimental data within uncertainties, whereas TALYS predictions were underestimated by a factor of 2 in the proton energy range of 37–45 MeV. For ^{69}Ge, our data agreed with TALYS and were slightly lower compared to the literature data. In both cases of Ge radioisotopes, only single experimental literature data were available for comparison. Regarding ^{66}Ga, our data agreed with [17] data and were slightly higher compared to TALYS predictions.

The discrepancy may be attributed to a lack of experimental data. Since the predictions are also subject to uncertainty, achieving accurate estimations is challenging. The TALYS predictions are based on nuclear models and the cross-section database for nuclear reactions. Increased experimental nuclear data enhances the accuracy of these predictions.

The experimental data from this study hold significant implications for advancing medical radionuclide production, particularly for radionuclide generators such as ^{68}Ge/^{68}Ga. The accurate cross-section measurements for ^{68}Ge provide critical insights into optimizing the irradiation parameters for its production. Specifically, this data can fine-tune the proton energy range to maximize yield and minimizing radioimpurities, thus enhancing the efficiency of ^{68}Ge/^{68}Ga generators widely used in PET.

Furthermore, the detailed excitation functions for germanium isotopes enable more informed decisions regarding target material selection and thickness. For example, natural germanium targets, as investigated in this work, present a cost-effective alternative to enriched targets for certain applications, particularly in facilities where beam energy is well controlled.

These results also have broader implications for improving production methodologies in industrial and medical facilities. By providing a more comprehensive database for proton-induced reactions on germanium, this study supports the development of advanced cyclotron-based production systems. Such systems can cater to the growing demand for radionuclides in diagnostic and therapeutic applications, particularly in regions with limited access to reactor-based isotopes.

Data availability statement

All data that support the findings of this study are included within the article (and any supplementary files).

ORCID iDs

Arshiya Anees Ahmed https://orcid.org/0000-0003-1187-7417
Kamil Brudecki https://orcid.org/0000-0003-2677-4859
Barbara Marczewska https://orcid.org/0000-0001-5272-0948

References

[1] Vertes A, Nagy S, Klencsar Z, Lovas R G and Rosch F 2011 *Handbook of Nuclear Chemistry* vol 1 (Springer) (https://doi.org/10.1007/978-1-4419-0720-2)
[2] Global Cancer Facts and Figures—American Cancer Society, Online available: https://www.cancedsr.org/research/cancer-facts-statistics/global-cancer-facts-and-figures.html#:/:text=According%20to%20estimates%20from%20the,9.5%20million%20cancer%20deaths%20worldwide%
[3] Cancer rates by Human Development Index -World Cancer Research Fund International. Online Available: https://www.wcrf.org/cancer-trends/cancer-rates-human-development-index/
[4] Qaim S M 2017 Nuclear data for medical applications: an overview of present status and future needs *EPJ. Web. Conf.* **146** 08001
[5] Levkovskij V N 1991 Activation cross sections for the nuclides of medium mass region (A = 40–100) with protons and alpha-particles at medium (E = 10–50 MeV) energies (Experiment andsystematics), INTER-VESTI, Moscow, Russia
[6] Blosser H G and Handley T H 1955 Survey of (p, n) reactions at 12 MeV *Phys. Rev.* **100** 1340–4

[7] Barrandon J, Debrun J, Kohn A and Spear R 1975 tude du dosage de Ti, V, Cr, Fe, Ni, Cu et Zn par activation avec des protons d'nergie limite a 20 MeV *Nucl. Instrum. Methods* **127** 269–78
[8] Uddin M, Khandaker M, Kim K, Lee Y and Kim G 2007 Excitation functions of the proton induced nuclear reactions on ^{nat}Zn up to 40 MeV *Nucl. Instrum. Methods Phys.* B **258** 313–20
[9] Asad A H, Chan S, Morandeau L, Cryer D, Smith S V and Price R I 2014 Excitation functions of ^{nat}Zn(p,x) nuclear reactions with proton beam energy below 18 MeV *Appl. Radiat. Isot.* **94** 67–71
[10] Blaser J P, Boehm F, Marmier P and Peaslee D C 1951 Fonctions dexcitation de la reaction (p, n) *Helv. Phys. Acta* **24** 3–38
[11] Howe H A 1958 (p, n) cross sections of copper and zinc *Phys. Rev.* **109** 2083–5
[12] Hille M, Hille P, Uhl M and Weisz W 1972 Excitation functions of (p, n) and (α, n) reactions on Ni, Cu and Zn *Nucl. Phys.* A **198** 625–40
[13] Little F E and Lagunas-Solar M C 1983 Cyclotron production of ^{67}Ga. Cross sections and thick-target yields for the ^{67}Zn(p, n) and ^{68}Zn (p, 2n) reactions *Int. J. Appl. Radiat. Isot.* **34** 631–7
[14] Kopeck P 1990 Cross sections and production yields of 66Ga and 67Ga for proton reactions in natural zinc *Int. J. Radiat. Appl. Instrum.* A **41** 606–8
[15] Trknyi F, Szelecsnyi F, Kovcs Z and Sudr S 1990 Excitation functions of proton induced nuclear reactions on enriched ^{66}Zn, ^{67}Zn and ^{68}Zn production of ^{67}Ga and ^{66}Ga *Radiochim. Acta* **50** 19–26
[16] Hermanne A, Walravens N and Cicchelli O 1992 Optimization of isotope production by cross section determination *Int. Conf. on Nucl. Data for Sci. and Technol., Juelich* p 616–8
[17] Nortier F, Mills S and Steyn G 1991 Excitation functions and yields of relevance to the production of ^{67}Ga by proton bombardment of ^{nat}Zn and natge up to 100 MeV *Int. J. Radiat. Appl. Instrum.* A **42** 353–9
[18] Szelecsnyi F, Boothe T E, Tavano E, Plitnikas M E, Feijoo Y, Takcs S, Trknyi F and Szucs Z 1994 New cross section data for 66–67–68 Zn+p reactions up to 26 MeV *Int. Conf. Nucl. Data for Science and Technology, Gatlinburg, Tennessee, USA* p 393
[19] Szelecsnyi F, Boothe T E, Takcs S, Trknyi F and Tavano E 1998 Evaluated cross section and thick target yield data bases of zn+p processes for practical applications *Appl. Radiat. Isot.* **49** 1005–32
[20] Szelecsnyi F, Kovcs Z, van der Walt T, Steyn G, Suzuki K and Okada K 2003 Investigation of the ^{nat}Zn(p, x)^{62}Zn nuclear process up to 70 MeV: a new ^{62}Zn/^{62}Cu generator *Appl. Radiat. Isot.* **58** 377–84
[21] Szelecsnyi F, Steyn G, Kovcs Z, van der Walt T, Suzuki K, Okada K and Mukai K 2005 New cross-section data for the ^{66}Zn(p, n)^{66}Ga, ^{68}Zn(p, 3n)^{66}Ga, ^{nat}Zn(p, x)^{66}Ga, ^{68}Zn(p, 2n)^{67}Ga and ^{nat}Zn(p, x)^{67}Ga nuclear reactions up to 100 MeV *Nucl. Instrum. Methods Phys. Res.* B **234** 375–86
[22] Al-Saleh F S, Al Mugren K S and Azzam A 2007 Excitation function measurements and integral yields estimation for ^{nat}Zn(p, x) reactions at low energies *Appl. Radiat. Isot.* **65** 1101–7
[23] McGee T, Rao C, Saha G and Yaffe L 1970 Nuclear interactions of ^{45}Sc and ^{68}Zn with protons of medium energy *Nucl. Phys.* A **150** 11–29
[24] Johnson C H, Trail C C and Galonsky A 1964 Thresholds for (p, n) reactions on 26 intermediate-weight nuclei *Phys. Rev.* B **136** 1719–29
[25] Antropov A E, Gusev V P, Zhuravlev Y Y, Zarubin P P, Kolozhvary A A and Smirnov A V 1992 Total cross sections of (p, n) reaction on the nuclei of isotopes nickel and zinc at $E(p) = 5$–6 MeV *J, IZV* **56** 198
[26] Szelecsnyi F, Kovcs Z, Nagatsu K, Fukumura K, Suzuki K and Mukai K 2012 Investigation of direct production of ^{68}Ga with low energy ultiparticle accelerator *Radiochim. Acta* **100** 5–11
[27] Kotelnikova G, Lovchikova G, Sal'nikov O, Simakov S, Trufanov A and Fetisov N 1980 The investigation of neutron energy spectra for ^{68}Zn(p,n)^{68}Ga reaction *Report No. 1141* Fiz.-Energ. Institut. Obninsk
[28] Esat M T, Spear R H, Zyskind J L, Shapiro M H, Fowler W A and Davidson J M 1981 Test of global hauser-feshbach calculations for proton-induced reactions on ^{68}Zn *Phys. Rev.* C **23** 1822–5
[29] Vinogradov V, Zhuravlev Y, Zarubin P and Kolozhvari A 1993 Excitation functions of (p, n) reactions on zinc isotopes in the range of $E(p)$ from 4.9 to 5.9 MeV *Izv. Rossiiskoi Akademii Nauk, Ser. Fiz.* **57** 154–9

[30] Zhuravlev P Y, Zarubin Y P, Zeic Y V, Kolozhvari A A and Chelgunov I V 1995 Excitation functions of (p, n) reactions on nuclei of isotopes Zn from $E(p) = 5.6$ to 6.8 MeV *Izv. Rossiiskoi Akademii Nauk* **59** 118
[31] Hermanne A, Adam-Rebeles R, Trknyi F, Takcs S and Ditri F 2015 Proton and deuteron induced reactions on natga: experimental and calculated excitation functions *Nucl. Instrum. Methods Phys.* B **359** 145–54
[32] Cohen B L, Newman E and Handley T H 1955 (p, pn) + (p, 2n) and (p, 2p) cross sections in medium weight elements *Phys. Rev.* **99** 723–7
[33] Porile N, Tanaka S, Amano H, Furukawa M, Iwata S and Yagi M 1963 Nuclear reactions of Ga^{69} and Ga^{71} with 1356 MeV protons *Nucl. Phys.* **43** 500–22
[34] Adam-Rebeles R, Hermanne A, den Winkel P V, Vis L D, Waegeneer R, Trknyi F, Takcs S and Takcs M P 2013 ^{68}Ge/^{68}Ga production revisited: excitation curves, target preparation and chemical separation purification *Radiochim. Acta* **101** 481–9
[35] Humes R M, Dell G F, Ploughe W D and Hausman H J 1963 (p, n) cross sections at 6.75 MeV *Phys. Rev.* **130** 1522–4
[36] Basile D, Birattari C, Bonardi M, Goetz L, Sabbioni E and Salomone A 1981 Excitation functions and production of arsenic radioisotopes for environmental toxicology and biomedical purposes *Int. J. Appl. Radiat. Isot.* **32** 403–10
[37] Horiguchi T, Kumahora H, Inoue H and Yoshizawa Y 1983 Excitation function of Ge(p, $xnyp$) reactions and production of ^{68}Ge *Int. J. Appl. Radiat. Isot.* **34** 1531–5
[38] Spahn I, Steyn G, Nortier F, Coenen H and Qaim S 2007 Excitation functions of ^{nat}Ge(p, xn)^{71,72,73,74}As reactions up to 100 MeV with a focus on the production of ^{72}As for medical and ^{73}As for environmental studies *Appl. Radiat. Isot.* **65** 1057–64
[39] Mushtaq A, Qaim S and Stcklin G 1988 Production of ^{73}Se via (p, 3n) and (d, 4n) reactions on arsenic *Int. J. Radiat. Appl. Instrum.* A **39** 1085–91
[40] DeGraffenreid A J, Medvedev D G, Phelps T E, Gott M D, Smith S V, Jurisson S S and Cutler C S 2019 Cross-section measurements and production of ^{72}Se with medium to high energy protons using arsenic containing targets *Radiochim. Acta* **107** 279–87
[41] Fox M B *et al* 2021 Measurement and modeling of proton-induced reactions on arsenic from 35 to 200 MeV *Phys. Rev.* C **104** 064615
[42] Fabender M, de Villiers D, Nortier M and van der Walt N 2001 The ^{nat}Br(p, x)^{73,75}Se nuclear processes: a convenient route for the production of radioselenium tracers relevant to amino acid labelling *Appl. Radiat. Isot.* **54** 905–13
[43] de Villiers D, Nortier M and Richter W 2002 Experimental and theoretical excitation functions for ^{nat}Br(p,x) reactions *Appl. Radiat. Isot.* **57** 907–13
[44] Meija J *et al* 2016 Isotopic compositions of the elements 2013 (iupac technical report) *Pure Appl. Chem.* **88** 293–306
[45] Hermanne A *et al* 2019 Reference cross sections for charged-particle monitor reactions *Nucl. Data Sheets* **148** 338–82
[46] Brun R and Rademakers F 2022 Root: data analysis framework, version 6.26/08, https://root.cern/
[47] 2020 Nuclear structure and decay data, https://www-nds.iaea.org/relnsd/vcharthtml/VChartHTML.html
[48] National Nuclear Data Center, Brookhaven National Laboratory publication date unknown, https://www.nndc.bnl.gov/
[49] Chu S Y F, Ekström L P and Firestone R B 1999 Table of Radioisotopes Version 2.0 The Lund/LBNL Nuclear Data Search, https://nucleardata.nuclear.lu.se/toi/index.asp
[50] Ahmed A A, Wrońska A, Magiera A, Curcio A, Jaglarz M and Wawrzyniak A 2020 Study of ^{99}Mo and long-lived impurities produced in the ^{nat}Mo(γ, x) reactions using an electron beam *Radiat. Phys. Chem.* **177** 109095
[51] 2023 Talys (software), version 2.0
[52] Experimental nuclear reaction data (EXFOR). Database version of June 2024, https://www-nds.iaea.org/exfor/exfor.htm
[53] Trknyi F, Ditri F, Csikai J, Takcs S, Uddin M, Hagiwara M, Baba M, Shubin Y and Dityuk A 2005 Activation cross-sections of long-lived products of proton-induced nuclear reactions on zinc *Appl. Radiat. Isot.* **62** 73–81
[54] Jennewein M, Schmidt A, Novgorodov A F, Qaim S M and Rsch F 2004 A no-carrier-added ^{72}Se/^{72}As radionuclide generator based on distillation *Radiochim. Acta* **92** 245–9

[55] Jennewein M, Qaim S M, Kulkarni P V, Mason R P, Hermanne A and Rsch F 2005 A no-carrier-added ^{72}Se/^{72}As radionuclide generator based on solid phase extraction *Radiochim. Acta* **93** 579–83

[56] Jennewein M *et al* 2005 A new method for radiochemical separation of arsenic from irradiated germanium oxide *Appl. Radiat. Isot.* **63** 343–51

[57] Gmez-Batista M, Metian M, Teyssie J-L, Alonso-Hernndez C and Warnau M 2007 Bioaccumulation of dissolved arsenic in the oyster crassostrea virginica: a radiotracer study *Environ. Bioindic.* **2** 237–44